

CORROSION AND CONTAMINANT DIFFUSION MULTI-PHYSICS MODEL FOR COPPER-ALUMINUM WIREBONDS IN HIGH TEMPERATURE HIGH HUMIDITY ENVIRONMENTS

Pradeep Lall and Yihua Luo
Auburn University
NSF-CAVE3 Electronics Research Center
Department of Mechanical Engineering
Auburn, AL, USA
lall@auburn.edu

Luu Nguyen
Texas Instruments, Inc,
Santa Clara, CA, USA

ABSTRACT

Copper aluminum interconnects are being used in automotive applications for deployment underhood, on-engine and on-transmission. Electronics is widely used for enabling safety function including lane departure warning systems, collision avoidance systems, antilock braking systems, and vehicle stability systems. Models for copper interconnect degradation are needed for life prediction modeling to ensure 10-year, 100,000 mile reliability for electronics in automotive applications. Small concentrations of chloride ions may diffuse towards the bond pad interface under temperature, humidity, and electrical bias. The chloride ions may act as a catalyst breaking down the passivation layer of aluminum pad and accelerate the micro-galvanic corrosion at the copper-aluminum leading to the failure of the wirebond. Models for prediction of the diffusion of the chloride ions and the corrosion of the copper-aluminum interface have been difficult to develop, because of the small scale of the interface and the lack of appropriate electro-chemical properties for the Cu-Al system and the Electronic Molding Compounds under conditions relevant to operation. In this effort, a multiphysics model for galvanic corrosion in the presence of chloride has been presented. The contaminant diffusion along with the corrosion kinetics has been modeled. In addition, contaminated samples with known concentration of KCl contaminant have been subjected to the temperature humidity conditions of 130°C/100RH. The resistance of the Cu-Al interconnects in the PARR test have been monitored periodically using resistance spectroscopy. The diffusion coefficients of chloride ion has been measured in the electronic molding compound at various temperatures using two methods including diffusion cell and inductively coupled plasma (ICPMS). Moisture ingress into the EMC has been quantified through measurements of the weight gain in the EMC as a function of time. Tafel parameters including the open circuit potential and the slope of the polarization curve has been measured for both copper, aluminum under different concentrations of the ionic species

and pH values in the EMC. The measurements have been incorporated into the COMSOL model to predict the corrosion current at the Cu-Al bond pad. The model predictions have been correlated with experimental data.

INTRODUCTION

Copper wire has the advantages of the lower cost, lower thermal resistivity, lower electrical resistivity, higher mechanical strength and higher deformation stability over the gold wire. In spite of the upside above, the Cu-Al wire bond is susceptible to the galvanic corrosion and the reliability of Cu-Al wire bond is of great concern. Typical electronic molding compounds are hydrophilic and absorb moisture when exposed to humid environmental conditions. EMC may contain ionic contaminants including chloride ions as a result of the chemical synthesis of the subcomponents of the resin, etching of metallization, the decomposition of the die-attach, epichlorohydrin in the resin as a flame retardant. The presence of moisture in the operating environment of semiconductor package makes the ion more mobile in the EMC. The migration of chloride ions to the Cu-Al interface may induce galvanic corrosion inside the package causing degradation of the bond interface resulting in eventual failure. The rate at which the corrosion happens in the microelectronic packages is dependent upon the rate at which the ions transport through the EMC in addition to the reaction rate at the interface.

Past research has shown that formation of excessive intermetallics at Cu-Al interface is a major contributor to failure of the wire bond accompanied by resistance increase and fracture or bond lifts [Boettcher 2011; England 2011]. Past researchers have studied the IMC growth under isothermal aging. IMC has been studied using various techniques, including the crystal structure, effect of annealing time and effect of temperature on IMC growth [Na 2011]. Composition of IMC has been studied using TEM and XRD, and reported to be CuAl_2 and Cu_9Al_4 [Wieczorek-Ciurowa 2005; Laik 2008; Lee 2005]. Previous

studies have reported that galvanic corrosion at the bond pad interface is the underlying cause of failure under HAST [Liu 2011; Kim 2010]. The Chlorine (Cl⁻) content level and the type of flame retardant have been found to significantly affect the reliability performance of Cu-Al wire bond [Seki 2010; Gan 2014]. However, a multiphysics model based on the fundamental material measurements of the diffusion characteristics of the ionic species and the corrosion kinetics of the copper-aluminum intermetallics is presently not available. In this paper, fundamental diffusion behavior of the ionic species has been measured in electronic molding compounds using two different methods including - inductively coupled plasma mass spectrometry and diffusion cell across an EMC barrier. In addition, the Tafel-Parameters, including the open-circuit potential and the slope of the polarization curves for the anodic and cathodic regions have been measured for both copper and aluminum under a variety of molar concentration of the ionic species and variety of pH values. The measured values have been used to simulate corrosion of Cu-Al wirebonds in COMSOL™. The model predictions have been correlated with experimental data from Parr Bomb tests of Cu-Al wirebond packages.

TEST VEHICLE

Cu-Al Semiconductor Packages

The test vehicle used for the study is the 32-pin chip scale package. The package is 4.5 mm in length, 5.5 mm in width, 0.7 mm in height. Each pin has a length of 0.45 mm and width of 0.3 mm.

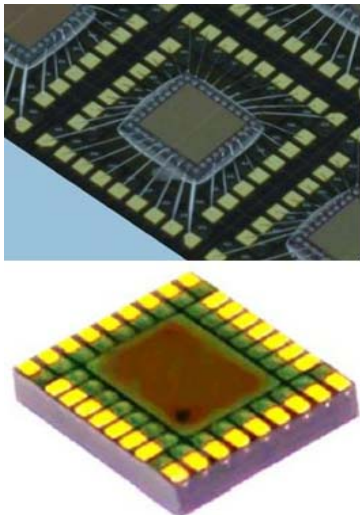


Figure 1: 32pin Chip Scale Package

The package interconnects has an I/O pitch of 0.5 mm. The package has 30µm diameter copper wires and aluminum pads. The packages used for the study were not daisy chained.. Figure 1 shows the optical microscopic images of the package inside and bottom.

Bulk Mold Compound Samples

Bulk molding compound samples with a thin square shape has been used for measurement of the diffusion characteristics of the chloride ions. The size of the samples

is representative of the dimensions used in area-array semiconductor packages. Samples length ranges from 42mm to 45mm as shown in Figure 2. Sample thickness ranges from 0.5mm to 1mm.

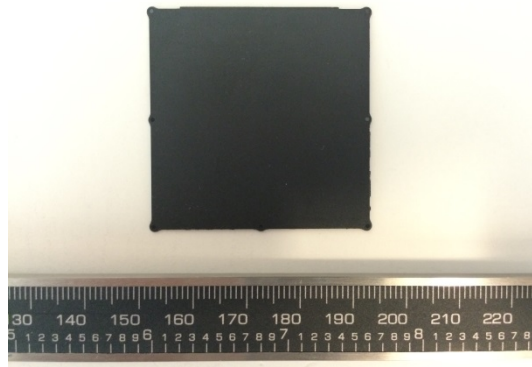


Figure 2: Representative Molding compound sample F

Sample materials are labeled as A, B, C, D, E and F. Molding compound A is a multi-aromatic epoxy. Molding compound B is an epoxy-phenol with a new resin. Molding compound C is a new non-epoxy resin. Molding compound D is a high temperature epoxy molding compound. Molding compound E is a silicone encapsulation material capable of high electrical resistivity, high thermal and mechanical stability and molding compound F is also a new type of resin providing superior performance with low warpage, low wire sweep, and high moisture reliability.

APPROACH

Two methods have been used to measure the diffusion coefficients of the chloride-ions in the electronic molding compound samples including – (a) diffusion cell (b) inductively coupled plasma. Details on the test parameters are described in the sections below.

Diffusion Cell Measurement

The diffusion cell consists of a stopper, two glass chambers, a clamp, two Styrofoam washers and a pedestal (Figure 3). The electronic molding compound sample has been used as a membrane between the two chambers of the diffusion cell. The epoxy molding compound sample is positioned in the 0.2cm² orifice between the upper donor chamber which has the volume capacity of 5ml and the lower chamber. The upper chamber is filled with 1M potassium chloride (KCl) solution. The lower chamber is the receptor chamber which has 5ml deionized water. The concentration-gradient across the interface of the electronic mold compound interface causes the chloride-ion diffusion from the KCl chamber to the deionized water chamber. A clamp and the two washers have been used to prevent the leakage at the orifice-mold compound interface. The top chamber is sealed with stopper and paraffin film to prevent the vaporization of KCl. The complete setup is placed vertically on a pedestal. The concentration of the chloride-ions in the deionized water chamber increases with time due to the concentration gradient between the chambers. The change in the concentration of chloride ions has been measured with

respect to time and used to calculate the diffusion coefficient of the EMC.



Figure 3: Diffusion Cell Setup



Figure 4: pH meter

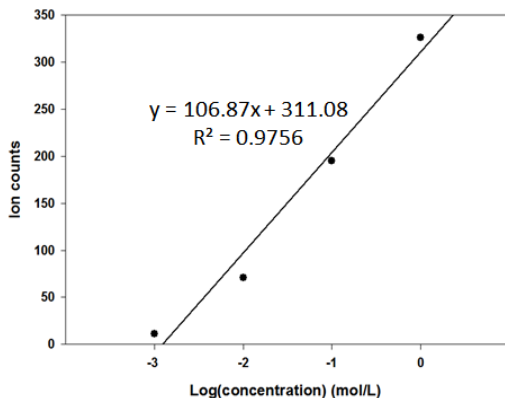


Figure 5: Calibration Plot

The 1M potassium chloride solution has been formulated using a laboratory grade powder. Potassium hydroxide and hydrochloric acid has been added to the solution in order to adjust the pH value to the desired level. Both temperature and the pH value will influence the ionic diffusion rate, thus the experiments have been performed at different temperatures values. A Cole-Parmer pH meter has been used to monitor the pH value (Figure 4) and the ionic

concentration has been measured using the Q-TOF mass spectrometer manufactured by Waters. The Q-TOF Premier is a hybrid orthogonal acceleration Time-of-Flight mass spectrometer that enables automated exact mass measurement of precursor and fragment ions. Before actually measuring the concentration of chloride ion in solutions, a calibration process is conducted in order to minimize the experiment error. During this process, four tubes of potassium chloride solution with different known concentrations are made. In each of the four test tubes, 1ml of solution has been moved from the test tube into the testing vial where the solutions are going to be tested. The result of the test gives the chloride ion counts of the corresponding 1ml solutions. The plot of ion counts as a function of the logarithmic values of the corresponding concentrations is shown in Figure 5. Once this step is done, the subsequent ion counts measurements are converted to the ionic concentrations simply by using this linear regression model. Fick's law of diffusion is used to describe the ionic diffusion [Simon 2004] and solve for the diffusion coefficient D in m^2/s . The original model has been simplified, resulting in a one-dimensional diffusion model based on the assumption that the ionic diffusion along length and width of EMCs are both negligible because of the uniformity of the concentration along the length and width of the sample and the small thickness of the samples.

Given the Fick's law $J = -D(dc/dx)$ where J is the ionic flux in moles/ $m^2 \cdot s$, c is the ionic concentration in moles/L, x is the variable in the thickness direction of the EMC sample. The diffusion coefficient is calculated by substituting the measured values of the chloride ion concentration from the receptor chamber, time of observation, and the thickness of the EMC sample into the equation for Fick's Law as shown below:

$$J = -D(dc/dx) \tag{1}$$

Dimensionally,

$$\left[\frac{\text{mol}}{m^2 \cdot s} \right] = \left[\frac{m^2}{s} \right] \left[\frac{\text{mol}/m^3}{m} \right] \tag{2}$$

Ionic flux has been calculated using data measured at $t = 5.18 \times 10^5$ sec, orifice area, $a = 2 \times 10^{-5} m^2$, receptor chamber concentration $c = 1.77 \times 10^{-3} \text{ mol/L}$, receptor chamber volume of $v = 5 \text{ ml} = 5 \times 10^{-3} \text{ L}$. The ionic flux has been calculated, as

$$J = \frac{\left(1.77 \times 10^{-3} \frac{\text{mol}}{\text{L}} \right) \left(5 \times 10^{-3} \text{ L} \right)}{\left(2 \times 10^{-5} m^2 \right) \left(5.18 \times 10^5 s \right)} = 8.54 \times 10^{-7} \frac{\text{mol}}{m^2 \cdot s} \tag{3}$$

The diffusion coefficient is calculated as,

$$D = \frac{8.54 \times 10^{-7} \frac{\text{mol}}{\text{m}^2 \text{s}}}{\frac{(1 - 1.77 \times 10^{-3})(10^3) \frac{\text{mol}}{\text{m}^3}}{5.3 \times 10^{-4} \text{m}}} = 4.54 \times 10^{-13} \frac{\text{m}^2}{\text{s}} \quad (4)$$

Similar calculations of diffusion coefficient have been done at various temperatures. Measurements demonstrate that the diffusion coefficient increases with the increase in ambient temperature (Figure 6). In Figure 6, the “dots” indicate the experimental measurements. The experimental data has been fit to an exponential model represented by the curve in Figure 6. Fit of the experimental data indicates activation energy of 46.8kJ/mol.

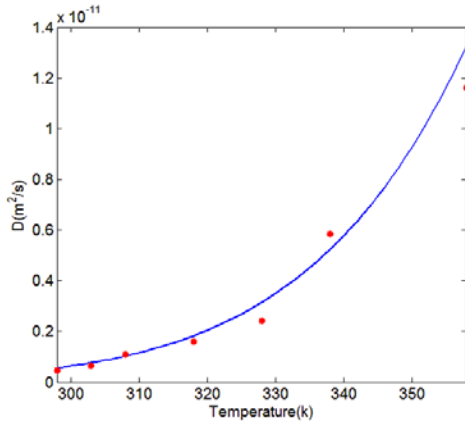


Figure 6: Diffusion Coefficient as a Function of T

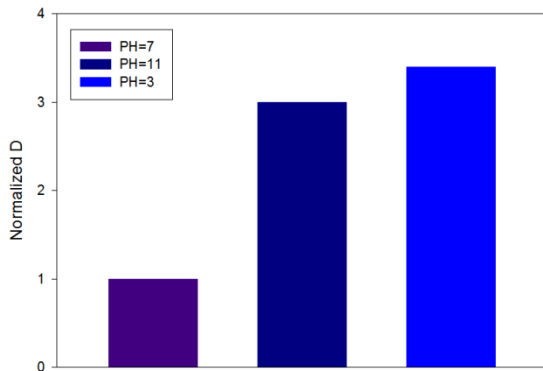


Figure 7: Comparison of Diffusion Coefficient Values under different PH values at room temperature

The diffusion coefficient has been measured under different pH values. Normalized value of the diffusion coefficient has been plotted versus the pH value in Figure 7. Diffusion coefficient has been assigned a value of 1 at the pH value of 7. The value of diffusion coefficient, D, at pH=3 and pH=11 are 3 times and 3.4 times as much as that of D at pH=7.

ICPMS-Based Diffusion Measurement

An alternative to the diffusion cell approach for the measurement of the diffusion coefficient is the inductively coupled plasma-based approach [Simon 2004]. The ICPMS has been used to cross-check the accuracy of the diffusion coefficient measured using the diffusion cell approach.

ICPMS is a tool for the determination of concentration of ionic species in a variety of different sample matrices. With this technique, solid samples are ashed by high temperature and then ashes are dissolved into a specific solution. After that, solution is injected into a radiofrequency (RF)-induced argon plasma using one of a variety of nebulizers. The sample mist reaching the plasma is quickly dried, vaporized, and energized through collisional excitation at high temperature. The atomic emission emanating from the plasma is viewed in either a radial configuration, collected with a lens or mirror, and imaged onto the entrance slit of a wavelength selection device. Single element measurements can be performed with a simple monochromatic tube combination. Simultaneous multi-element determinations are performed with the combination of a polychromatic and an array detector. In this experiment, several pieces of EMC sample are immersed into a 1M KCl solution beaker at a room temperature. The chamber with the 1M KCl solution was covered with aluminum foil to prevent water from evaporating. Samples are taken out periodically from the beaker. The retrieved samples are rinsed thoroughly with distilled water to remove any residual KCl solution on the surface and are ground and analyzed immediately using ICPMS as shown in Figure 8. Result of the analysis from the ICPMS is the average chloride-ion ingress from different aging hours in the EMC samples.

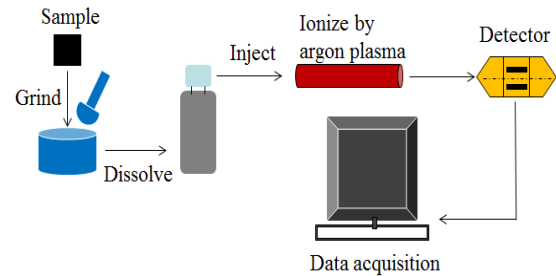


Figure 8: Schematic of ICPMS main processes

The test results have been used to calculate the diffusion coefficient of the EMC sample. For the purpose of computation of the diffusion coefficient, the diffusion of the KCl in the sample has been simulated in COMSOL Multiphysics. For the purpose of the analysis, the initial conditions assumed include a constant concentration of chloride-ions at the surface of the EMC sample while immersed in the 1M KCl solution. Since there is 35.543 AMU of chloride-ions per molecule of KCl, first, we have converted mol/L to to g/1000 g of solution, as follows:

$$\frac{1 \text{ mol}}{1 \text{ liter}} \cdot \frac{35.543 \text{ AMU}}{1 \text{ molecule}} \cdot \frac{1.66054 \times 10^{-24} \text{ grams}}{1 \text{ AMU}} \quad (5)$$

$$\frac{6.023 \times 10^{23} \text{ molecules}}{1 \text{ mol}} = 35.543 \frac{\text{grams}}{\text{liter}}$$

Where, 35.543 AMU is the atomic weight of the chloride-ion, one AMU is 1.66054×10^{-24} grams, and 6.023×10^{23} is the Avogadro’s Number. Since the density of water is 1

grams/ml, the concentration of chloride-ions can be converted to grams per 1000 grams of solution from the current units of grams per liter, as follows:

$$35.543 \frac{\text{grams}}{\text{liter}} = 35.543 \frac{\text{grams}}{1000 \text{ grams}} \quad (6)$$

The concentration has been converted to ppm by multiplying the numerator and the denominator by 1000, as follows:

$$35.543 \frac{\text{grams}}{1000 \text{ grams}} \quad (7)$$

$$= \frac{35.543 * 1000 \text{ grams}}{1,000,000 \text{ grams}} = 35,543 \text{ ppm}$$

For the initial conditions of the multiphysics model, it has been assumed that the chloride-ion concentration at the surface of the sample is 35,543 ppm. The concentration of the chloride ions obtained from ICPMS has been used for the concentration in the core of the EMC sample. The length and width of the sample is considerably greater than the sample thickness. Since, the concentration of the chloride ions is uniform on the surface of the sample, it is reasonable to assume one-dimensional diffusion through the thickness of the sample. Electric potential gradient is set to be zero because the lack of electrical field. Trial and error is used to calculate the diffusion coefficient of the chloride ion at room temperature. In addition to the steps above, the empirical equations provided by Shen, et. al. [1976] plotted and compared to the results of simulation in order to cross-check value of D:

$$c(t) = c_s \left[1 - \exp \left[-7.3 \left(\frac{D \cdot t}{h^2} \right)^{3/4} \right] \right] \quad (8)$$

In this equation, c(t) denotes the concentration at time t, c_s is the saturation level, and h is the thickness of the EMC sample.

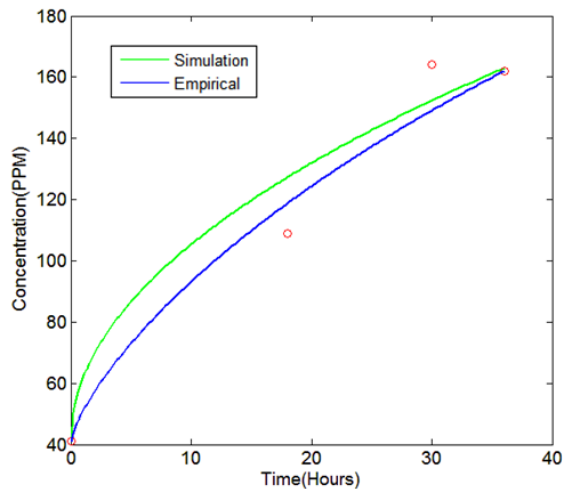


Figure 9: Comparison among Results of Multiphysics Simulation, Empirical Equation and Experiment results

From the plot above, it can be readily seen that the simulation results not only match the experiment data but also fit the empirical equation, the maximum error between experiment results and simulation results is 16.8%. As a result, diffusion coefficient of chloride ion under room temperature is acquired, which is $1.7 \cdot 10^{-13} \text{ m}^2/\text{s}$. The result acquired by this approach is approximately 2.5 times small than the D value calculated by the diffusion cell approach. As both results have the same orders of magnitude, the two previous approaches are considered to be suitable approaches to calculating the diffusion coefficient of chloride ion in the molding compound.

Scanning Electron Microscope and Energy-dispersive X-ray Spectroscopy Analysis

In this series of experiments, molding compound samples are aged in 1M potassium chloride solutions at different temperatures for different amount of time and the cross-section of samples are investigated by using the scanning electron microscope and energy-dispersive X-ray spectroscopy technologies after they are rinsed thoroughly with DI water. The instrument model used here is Zeiss EVO 50 series along with an Oxford INCA EDS X-ray Microanalysis System. Due to the complex formulation of epoxy molding compounds, the ionic diffusion paths inside EMCs are not as simple as that inside homogenous materials. Previously, there are two major assumptions of the ionic diffusion path in EMCs known as bulk ionic diffusion and interfacial ionic diffusion.

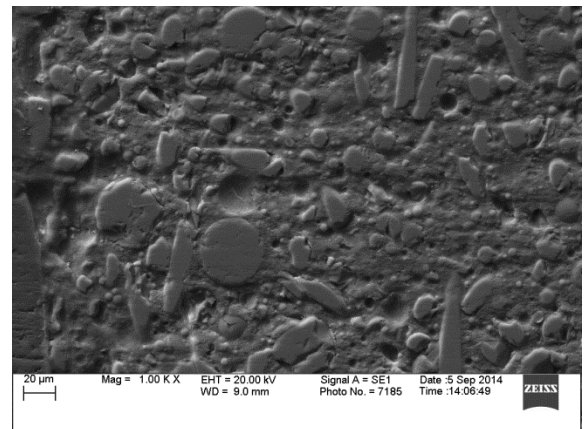


Figure 10: SEM Image of Cross-section of EMC Sample B after a 3-week immersion in 1M KCl Solution at 85°C

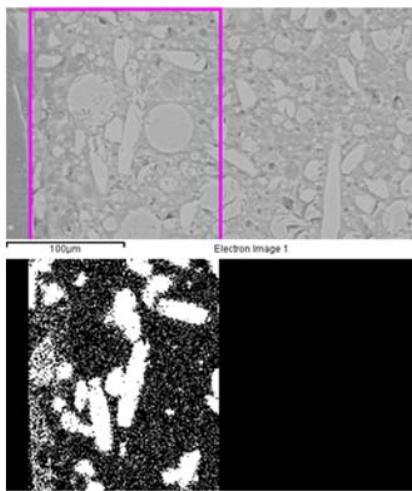


Figure 11: EDS Mapping Image of Figure 10

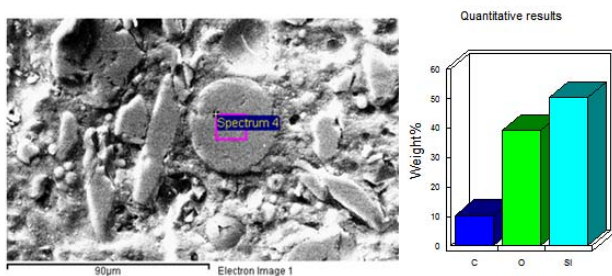


Figure 12: SEM Image and EDS Spot Analysis of Filler Material A

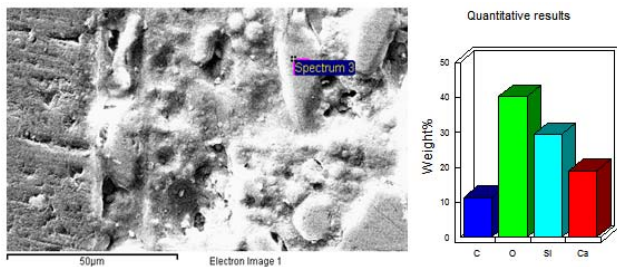


Figure 13: SEM Image and EDS Spot Analysis of Filler Material B

In bulk ionic diffusion, the ionic species travel through the matrix as opposed to the interfacial diffusion in which ionic species travel through the interfaces of the matrix and the filler materials. Figure 10 shows the microscopic view of EMC sample B after being aged in 1M KCl solution for three weeks at 85°C. As it can be seen readily from the image, this type of molding compound is filled with fillers that have two different shapes. One of which is round-shaped and the other is bar-shaped. In order to figure out the number of filler materials in the EMC, EDS mapping image is acquired from the left part of Figure 11. Analysis indicates a strong calcium signal at the white-colored part. This part is perfectly aligned with the bar-shaped filler material in the previous image which implies two things, there are two different types of filler materials in EMCs and one of them contains certain amount of element calcium.

Figure 12 and Figure 13 show the results of EDS spot analysis of both two filler materials. Both of the filler materials contain element carbon, oxygen and silicon. In addition to those aforementioned elements, Filler B contains an extra noticeable amount of calcium. Filler A shows a composition of round fused silica which is widely used in EMCs to impart the desired coefficient of thermal expansion, elastic modulus and fracture toughness properties. Filler B is composed of calcium carbonate that can enhance the thermal transfer property of the polymer. In an attempt to find out the diffusion mode of chloride ion, the chloride ion mapping image is obtained from the left part of Figure 10. It is observed that before the immersion process, the mapping signal of chloride ion is below the detection limit of the SEM/EDS instrument. However, after the immersion of the EMC sample in the 1M KCl solution, the mapping signal image of chloride ion is readily measurable. The chloride ion signal has been acquired and is overlapped with the image of Figure 10. The molding compound samples have been aged in 1M KCl solution at 85°C for 3 weeks. Figure 14 shows that signal of chloride ion in the image are strongest in the area closed to the edge and signal intensity decreases with increasing depth inside the EMC. This is in consistent with the fact that ionic ingress starts from the solution/EMC interface and proceeds into the sample due to the concentration gradient. Furthermore, investigation of the image below leads to the conclusions that ionic species tends to diffuse through the interfacial area particularly between the matrix and the calcium carbonate as there is almost no signal detected on the bar-shaped material and chloride signal is relatively stronger at the filler/matrix interface.

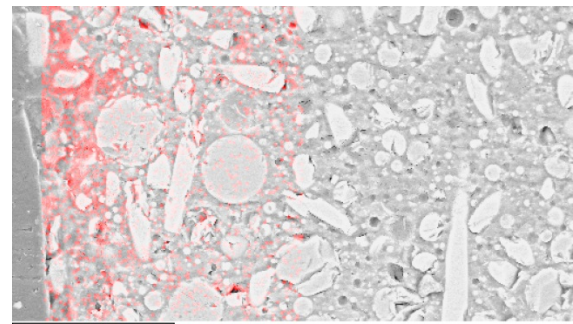


Figure 14: Image Overlap between Chloride Ion Mapping and cross-section of EMC Sample B

The results from the EDX analysis indicate that ionic diffusion inside EMC sample B is interfacial diffusion. More specifically, it diffuses around the calcium carbonate. The reason for this interfacial diffusion is probably because of the fact that there are micro-voids at the matrix/filler interface that allows moisture and ionic species to reside and it is easier for ionic species to diffuse through this interfacial path as this path has relatively the lowest diffusion resistance compared to the rest of the paths. A different set of 1M KCl solution immersion experiments have been performed on the EMC sample F at 150°C for 96 hours.

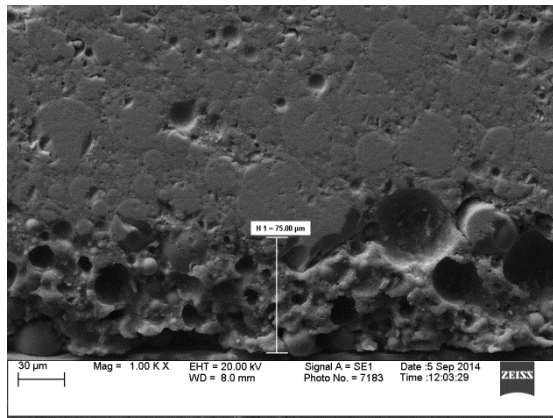


Figure 15: SEM Image of Cross-section of EMC Sample F after a 96-hour immersion in 1M KCl Solution at 150°C

Figure 15 shows that EMC type F has only one filler material of round fused silica. The EMC/solution interface degraded towards the center of the cross-section for about 75 micrometer due to the high temperature. From Figure 15, it can be readily seen that the degraded part has craters with different sizes, based on this special type of change of morphology and the fact that fused silica has high thermal stability, it can be concluded that the degradation is most likely caused by either the dissolution of epoxy resin or the reaction between epoxy resin and water around the edge at a high temperature. As a result, EMC could no longer hold on to the filler material because the loss of binding material.

Weight Loss Test

Weight loss tests were performed on all of the six-EMC samples. Prior to initiation of testing, the samples were baked at 130°C isothermal aging chamber for 72 hours to remove the moisture. Figure 16 shows that long-term exposure to very high temperature results in degradation of the binding material in molding compound which leads to the gradual loss of weight. Measurements indicate that EMC sample F has the biggest percentage weight loss after 2000 hour thermal aging while EMC sample D has the smallest one among all the six samples. The weight loss result is consistent with the intended use of the EMC sample D, which is a high temperature epoxy molding compound. Furthermore, the EMC sample F is a new type of resin providing superior performance with low warpage, low wire sweep, and high moisture reliability – thus intended for better reliability in humid environments.

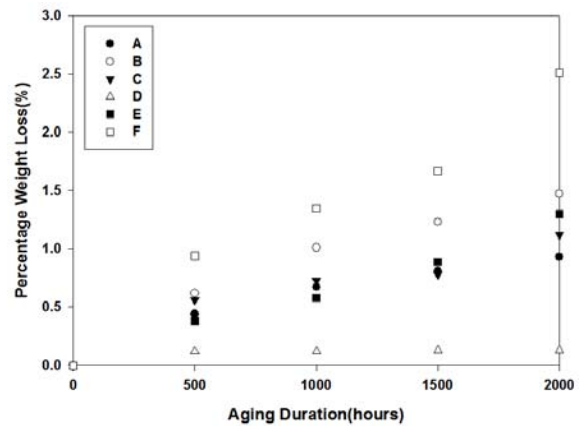


Figure 16: Weight Loss Test under 200°C

FTIR Test

Fourier transform infrared spectroscopy has been used to study the change of bonding structure of EMCs after long-term exposure to high temperature. The test samples used in this study have been aged in 175°C and 200°C chambers for 2000 hours. EMC samples were powdered and well-mixed with potassium bromide (KBr) powder to form pallet samples. Those samples are tested by Nicolet IR 100 and the corresponding data was transformed into spectrum. Next, the spectrums were compared to the KBr background spectrum to remove all the KBr peaks. Previously, researchers have used this technique to study the Effect of postcure on molding compound properties.

Electrochemical Polarization Test

Electrochemical polarization has been used to provide significant useful information regarding the corrosion rate and susceptibility of specific materials to corrosion in designated environments. Copper and aluminum samples were tested in solutions with different pH values and chloride ion concentrations to determine the effect of ionic-contaminants on corrosion behavior. Aluminum used for measurements was 6061 aluminum. Copper used for the study was 110 copper. The metal rod was cut into small pieces on which the electrical wire was soldered for the purpose of connection. The samples were encapsulated in epoxy resin in a manner to provide an exposed surface of the sample on one of the faces of the encapsulated assembly. The exposed surface was hand-polished with BUEHLER grinding paper up to 1200 grit and then degreased with ethanol, cleaned with distilled water and dried by air pump. Experiments were carried out in a conventional three-electrode electrochemical cell [Zaid 2008; Szklarska-Smialowska 1986] with a silver chloride reference electrode and a platinum counter electrode immediately after the sample preparation process in order to avoid prolonged exposure to air.

The Tafel curve has been used for the determination of the open-circuit potential, corrosion potential, or rest potential, E_0 . The slope of the Tafel curve provides the coefficient of charge transfer, γ . The data measured include the current-potential curve and the Tafel Curve [$\log_{10}(\text{current})$ vs

potential]. The current-potential curve follows the Butler-Volmer Equation for kinetic-controlled reaction [Bard, et. al. 2001, Pg 96; McCafferty 2010, Pg 138]:

$$i = nFAk_0 \left\{ -c_0 e^{\left[-\frac{\gamma nF}{RT}(E-E_0) \right]} + c_R e^{\left[(1-\gamma) \frac{nF}{RT}(E-E_0) \right]} \right\} \quad (9)$$

Where, γ is the charge transfer coefficient, n is the number of electrons transferred, F is the Faraday's Constant (9.6485×10^4 C/mol), T is the temperature (K), R is the gas constant (8.3145 J/mol.K), c_0 and c_R are the concentrations of the oxidant and reductant (moles/m²), k_0 is the reaction rate constant (sec⁻¹), E_0 is the electrode potential for zero current flow (also called the open-circuit potential, corrosion potential, or rest potential) in (volts), and A is the area (m²). The degree of polarization is defined as the overvoltage (or overpotential) η given by the difference $\eta = E - E_0$. The anodic slope corresponding to the positive overpotential is,

$$\frac{(1-\gamma)nF}{2.303 RT} \quad (10)$$

For the anodic portion of the curve, as α increases, the slope decreases. The slope of the cathodic region corresponding to the negative overpotential is,

$$\frac{\gamma nF}{2.303 RT} \quad (11)$$

It can be seen that as γ increases, the slope increases. The Tafel plot has been used to calculate the charge transfer coefficient, γ and the corrosion potential, E_0 . For the purpose of fitting the coefficients, Equation (9) has been expressed as follows:

$$j_{Cu} = j_{0Cu} \left\{ e^{\left(\frac{E_{Cu} - E_0}{\alpha_{Cu}} \right)} - e^{\left(-\frac{E_{Cu} - E_0}{\beta_{Cu}} \right)} \right\} \quad (12)$$

$$j_{Al} = j_{0Al} \left\{ e^{\left(\frac{E_{Al} - E_0}{\alpha_{Al}} \right)} - e^{\left(-\frac{E_{Al} - E_0}{\beta_{Al}} \right)} \right\} \quad (13)$$

Where, α_{Cu} is the anodic tafel-slope for copper, β_{Cu} is the cathodic tafel-slope for copper, α_{Al} is the anodic tafel-slope for aluminum, β_{Al} is the cathodic tafel-slope for aluminum, j_{0Al} is the current density in aluminum for zero over-potential, j_{0Cu} is the current density in copper for zero over-potential, E_{Cu} is the electrode potential for copper, E_{Al} is the electrode potential for aluminum, and E_0 is the open circuit potential. Samples were immersed in solutions

for 24-48 hours prior to the tests to attain stable open circuit potentials.

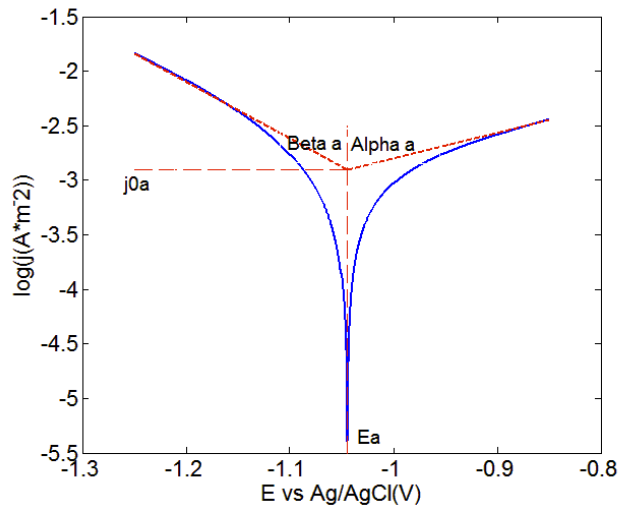


Figure 17: Schematic Plot of the Tafel Parameters

Table 1: Electrode Potential Difference between Copper and Aluminum in KCl solutions with Different pH values and Different Values of Ion Concentration

		pH = 3	pH = 7	pH = 11
KCl	0M	0.52 volt	0.75	0.38 volt
	0.01M	0.53 volt	0.95	0.52 volt
	0.5M	0.54 volt	1.02	0.62 volt

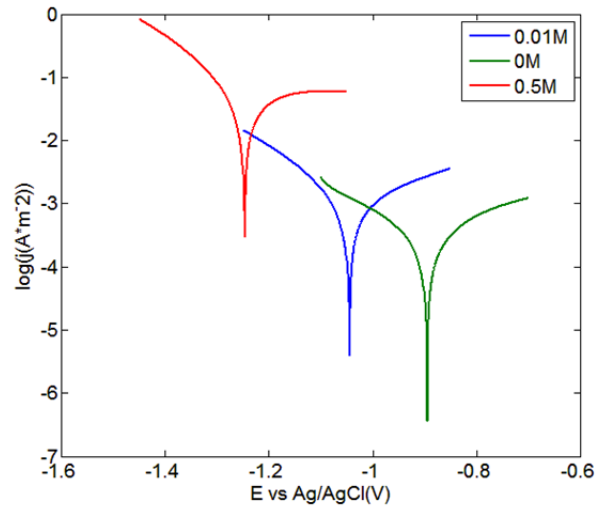


Figure 18: Polarization Curves of Copper under Different Values of Chloride Ion Concentration at pH=7

During the tests, the scan rate is set to 0.15mV/sec and the initial potential is set to at least 250mV below the OCP. Once the V-I curves were acquired, Tafel extrapolation method is used to fit curves to obtain Tafel parameters. From Table 1, it can be seen that the potential gap between copper and aluminum increases noticeably as the concentration of chloride ion increases in alkaline solution, which indicates an increasing likelihood of galvanic corrosion between two metals. As for acidic conditions, the

potential gap stays almost the same and the gap maintains at a relative high value. Figure 18 shows that as concentration of chloride ion increases, the standard potential of copper shifted to more negative values and the exchange current density increase drastically. From Figure 19, standard potential shifted to more negative when aluminum is immersed in a neutral solution and the current density stays unchanged as overpotential increases from 0.1V to 0.55V at pH=7. The same phenomenon didn't occur at the acidic and alkaline conditions. Under highly oxidizing and high concentration of chloride ion condition, passivation layer will be dissolved very quickly compared to that of neutral condition.

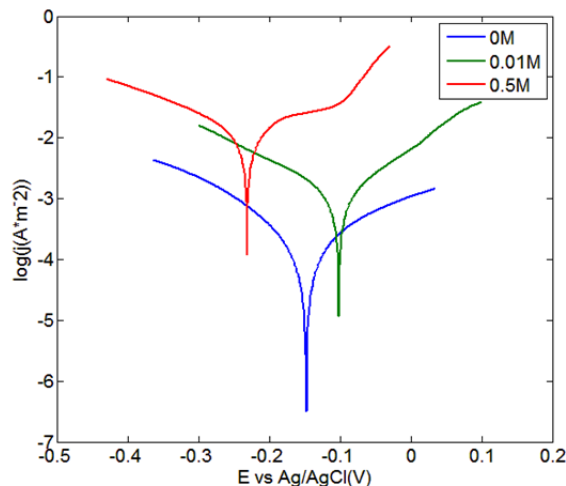


Figure 19: Polarization Curves of Aluminum under Different Values of Chloride Ion Concentration at pH=7

Table 2: Tafel Parameters – j_0 and Standard Potential, E_0

Cl ⁻ Ion Molarity	$j_0(\text{Al})$ ($\text{A}\cdot\text{m}^{-2}$)	$j_0(\text{Cu})$ ($\text{A}\cdot\text{m}^{-2}$)	$E_0(\text{Al})$ (vs Ag/AgCl) volts	$E_0(\text{Cu})$ (vs Ag/AgCl) volts
0M	0.0003	0.0001	-0.895	-0.147
0.01M	0.01	0.01	-1.044	-0.102
0.5M	0.05	0.04	-1.246	-0.231

Table 3: Tafel Parameters – α and β Slopes

Chloride-Ion Concentration	$\alpha(\text{Al})$	$\beta(\text{Al})$	$\alpha(\text{Cu})$	$\beta(\text{Cu})$
0M	0.3	0.3	0.25	0.25
0.01M	0.3	0.3	0.2	0.2
0.5M	0.2	0.2	0.18	0.18

The pitting corrosion potential coincides with the corrosion potential in acidic and alkaline solutions. Tafel parameters of both copper and aluminum were obtained at neutral condition under different values of KCl concentration and these parameters were used in the Butler-Volmer Equation for the simulation part to help calculate the dissolution rate of the aluminum pad in a copper aluminum wire bond system.

COMSOL SIMULATIONS

Micro-Galvanic Corrosion at Bond Pad Interface

This specific corrosion process initiates when two dissimilar metals (copper and aluminum) are electrically connected, and are in a conductive environment known as electrolyte (EMC). The corrosion is always associated with the presence of halide (chloride ion) as a catalyst. In the copper-aluminum wirebond, the aluminum part acts as anode and undergoes material dissolution while copper part acts as cathode where the reduction takes place (Figure 20). The electrons produced by the anodic reaction will be used by cathodic reaction.

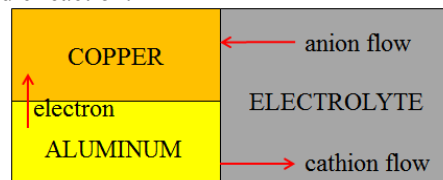


Figure 20: Schematic Plot of Galvanic Corrosion In this simulation, it is assumed that aluminum dissolution is the only anodic reaction and reduction is the only cathodic reaction.

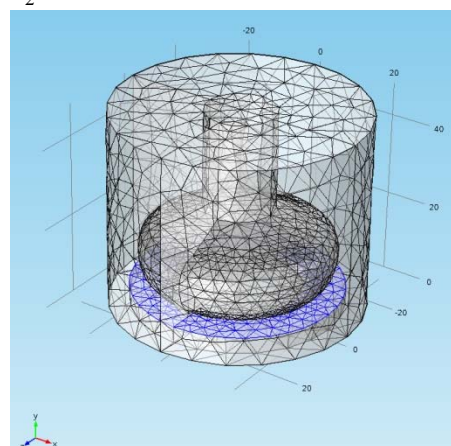


Figure 21: Model Geometry (unit in μm)

Figure 21 shows the simulation geometry, the cylindrical galvanic system is made of copper wire, ball bond and aluminum pad whose top surface is highlighted with blue. The radius of the ball bond is $25 \mu\text{m}$ and the thickness of aluminum pad is $0.75 \mu\text{m}$. The rest of the space is filled with epoxy molding compound.

Governing Equations and Subdomain Conditions

The net rate of electrode reaction is governed by the rate at which the electrochemical species is brought to the electrode surface:

$$v_{\text{erx}} = v_{\text{mt}} = \frac{i}{nFA} = \frac{j}{nF} \quad (16)$$

Where, v_{erx} is the net rate of electrode reaction ($\text{mol}\cdot\text{s}^{-1}\cdot\text{m}^{-2}$), v_{mt} is the rate at which the electrochemical species is

transferred to the electrode surface ($\text{mol}\cdot\text{s}^{-1}\cdot\text{m}^{-2}$), n is the stoichiometric number of electrons consumed in the electrode reaction (e.g., 3 for reduction of Al^{3+}), F is the Faraday's Constant, A is the area of the electrode (m^2), i is the current (amperes), j is the current density (A/m^2). The rate of mass transfer is proportional to the concentration gradient at the electrode surface and represented by:

$$v_{\text{mt}} = D_{\text{O}} \left(\frac{\partial C_{\text{O}}}{\partial x} \right)_{x=0} \quad (17)$$

Where, D_{O} is the diffusion coefficient for species O, and C_{O} is the concentration of species O. A linear concentration gradient has been assumed in the diffusion layer and represented by:

$$v_{\text{mt}} = D_{\text{O}} \left(\frac{C_{\text{O}}^* - C_{\text{O}(x=0)}}{\delta_{\text{O}}} \right) \quad (18)$$

Where, C_{O}^* is the bulk concentration, δ_{O} is the thickness of the diffusion layer. Since the thickness of the diffusion layer is not known, the diffusion coefficient and the diffusion layer thickness have been combined into a single constant:

$$v_{\text{mt}} = m_{\text{O}} [C_{\text{O}}^* - C_{\text{O}(x=0)}] = \frac{i}{nFA} \quad (19)$$

$$\frac{i}{nFA} = m_{\text{O}} [C_{\text{O}}^* - C_{\text{O}(x=0)}] \quad (20)$$

Information about the electrode reaction has been gained by determining the current as a function of potential and plotting the i - E curves. Departure of the electrode potential (E) from equilibrium potential (E_0) by passage of faradaic current (i) is termed as polarization. The extent of polarization is termed as the overpotential, $\eta = E - E_0$. The i - E curves are calculated from the Butler-Volmer Equation [Bard, et. al. 2001, Pg 96; McCafferty 2010, Pg 138]:

$$i = nFAk_0 \left\{ -c_0 e^{\left[-\frac{\gamma nF}{RT}(E-E_0) \right]} + c_R e^{\left[\frac{(1-\gamma)nF}{RT}(E-E_0) \right]} \right\} \quad (21)$$

Where, γ is the charge transfer coefficient, n is the number of electrons transferred, F is the Faraday's Constant ($9.6485 \times 10^4 \text{ C/mol}$), T is the temperature (K), R is the gas constant ($8.3145 \text{ J/mol}\cdot\text{K}$), c_0 and c_R are the concentrations of the oxidant and reductant (moles/m^3), k_0 is the reaction rate constant (sec^{-1}), E_0 is the electrode potential for zero current flow (also called the open-circuit potential, corrosion potential, or rest potential) in (volts), and A is the area (m^2). The degree of polarization is defined as the overvoltage (or overpotential) η given by the difference $\eta = E - E_0$. The values of α is the charge transfer coefficient and the open-circuit potential (E_0) previously measured using the polarization curves from the three electrode

electrochemical cell have been used for the simulation in COMSOL™. The movement of the chloride-ions due to diffusion, migration, and convection in the EMC is modeled with the Nernst-Planck Equation:

$$J_i = -D_i \nabla C_i - \frac{z_i F}{RT} C_i D_i \nabla \phi + C_i v \quad (22)$$

Where, J_i is the flux of species "i" ($\text{mol}\cdot\text{s}^{-1}\cdot\text{m}^{-2}$) at a specific distance from the surface, D_i is the diffusion coefficient (m^2/s), ∇C_i is the concentration gradient of species "i", $\nabla \phi$ is the potential gradient, z_i and C_i are the charge (dimensionless) and concentration ($\text{mol}\cdot\text{m}^{-3}$) of species "i", respectively, and $v(x)$ is the velocity (m/s) with which a volume element in solution moves along the axis. For the one dimensional case, the equation reduces to the following form,

$$J_i(x) = -D_i \frac{\partial C_i}{\partial x} - \frac{z_i F}{RT} C_i D_i \frac{\partial \phi}{\partial x} + C_i v \quad (23)$$

Nernst-Planck equation has been used to model the transport of ionic species in the EMCs. The driving force of the ionic transport is concentration gradient and electric gradient. The values of the diffusion coefficient (D) measured previously from ICPMS and diffusion cell have been used in the Nernst-Planck Equation. All the other boundaries are set to be insulating and no flux:

$$\vec{n} \cdot N_i = 0 \quad (24)$$

$$\partial \phi / \partial \vec{n} = 0 \quad (25)$$

Moving Boundary

In order to track the dissolution of aluminum pad and the effect of the dissolution on the corrosion current density, moving boundary condition is imposed on the aluminum pad. The pad dissolution rate is given by:

$$v = N_{\text{Al}^{3+}} M / \rho \quad (26)$$

Where v is the dissolution rate in the unit of m/s, M and ρ are molar mass and density of aluminum respectively. It is also assumed that only aluminum pad is subjected to free dissolution and the direction of it is along the negative y-axis.

SIMULATION RESULTS

Time dependent solver has been used to solve the multiphysics problem. Figure 22 shows the corrosion current density distribution prediction from the multiphysics model under zero concentration of chloride ion and neutral initial environmental condition. A higher corrosion current density correlates with a higher depletion rate of the aluminum pad. It can be readily seen from Figure 22 that the corrosion current density under the initial neutral and zero concentration of chloride-ions is in the neighborhood of 14mA. In addition, it can be seen that the distribution of corrosion current at the aluminum pad is nearly uniform with the inner ring of the pad in contact with the copper ball

bond exhibiting some variation in the corrosion current. Figure 23 shows the effect of local concentration of chloride ion on the corrosion current density. It can be readily seen that the corrosion current density is directly proportional to the chloride ion concentration.

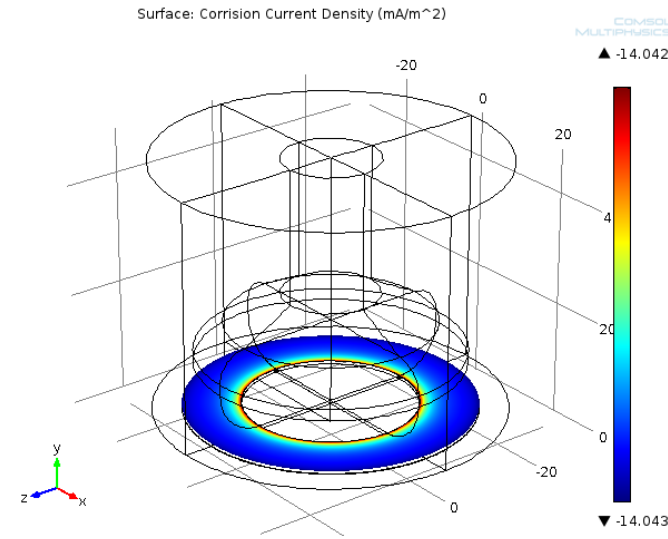


Figure 22: Time=0(Second)

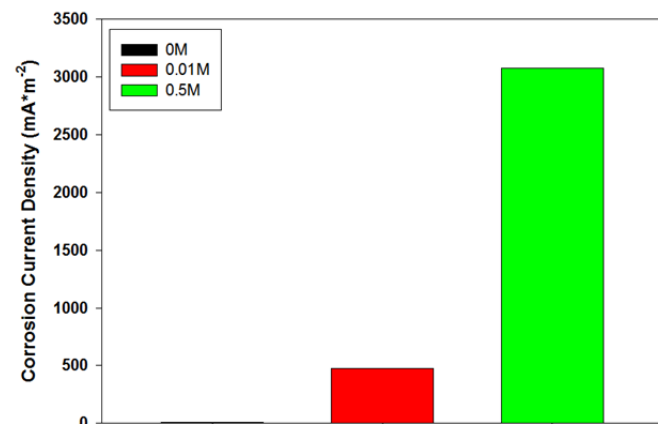


Figure 23: Average Corrosion Current Density

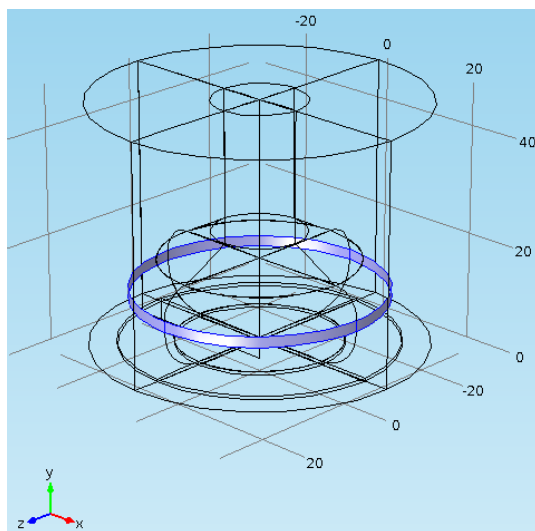


Figure 24: Hydroxide Ion Flux

For a chloride ion concentration of 0.01M, the correspond corrosion current density is 500 mA; for a chloride-ion concentration of 0.5M ionic concentration condition, the corresponding value of corrosion current density is 3000 mA. The corrosion rate increases dramatically as the concentration of chloride ion in the neighborhood of copper aluminum bond pad increases.

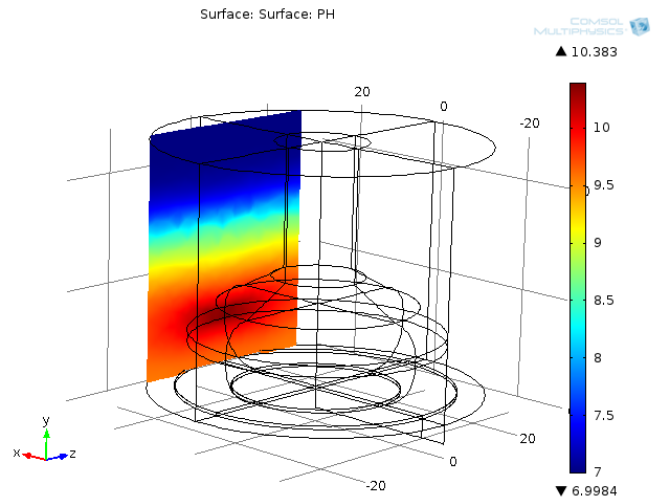


Figure 25: pH contour at time=10(hours)

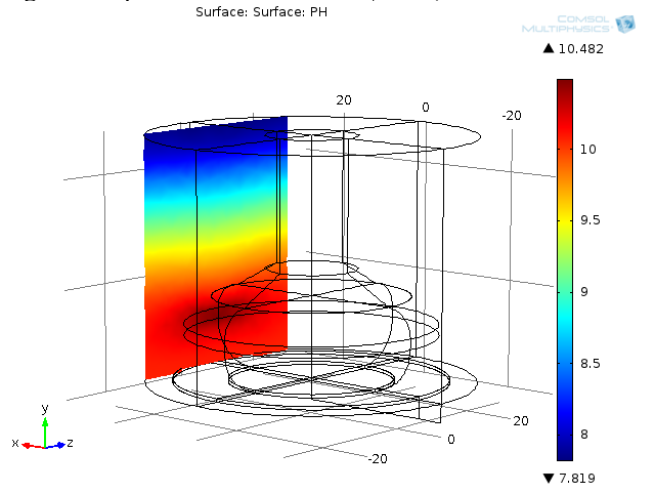


Figure 26: pH contour at time=24(hours)

The rate of peripheral material dissolution around a cathodic location is accelerated by alkaline attack due to the oxygen reduction reaction (ORR) or proton reduction occurring at the particle surface. Thus, the pH evolution in the vicinity of copper ball bond is of great interest. In the simulation, evolution of both hydrogen ion and hydroxide ion in the system are taken into account by adding an ionic flux at the copper/EMC interface which is highlighted with blue in Figure 24. The evolution of the pH values as a function of time is shown in Figure 25 at 10-hours and in Figure 26 at 24-hours on a plane located at the radius of the ball bond. This simulation has been run under initial neutral and zero concentration of chloride ion condition. Thus it can be concluded that the most alkaline part of the Cu-Al ball bond is the area in the vicinity of copper bond and as time proceeds, the alkalinity becomes stronger.

PACKAGE WITH BUILT-IN CONTAMINANT

In order to study how the KCl contaminant can affect the reliability of the Cu-Al wire bond based package, the package with built-in contaminant test is performed and the corresponding baseline samples are subjected to the same test condition of 130°C/100RH in a PARR bomb test chamber. The test was divided into three parts (Figure 27, Figure 28).

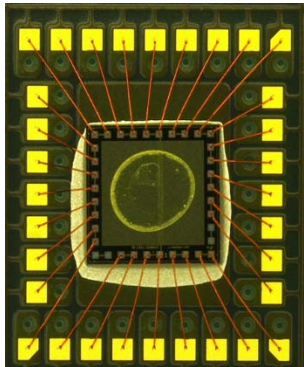


Figure 27: Optical microscopic sample image with built-in chloride contaminant

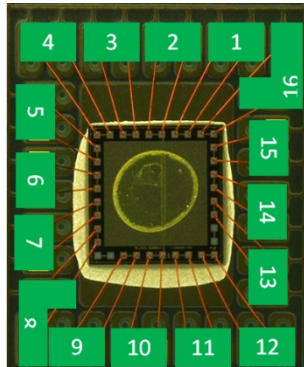


Figure 28: Sixteen pairs of wire bond has been labeled in order to measure and track change of resistances

# of PIN	Time zero	24 hr	48 hr	72hr	96hr	120hr
		130C/100 %RH parr bomb	130C/100 %RH parr bomb	130C/10 0%RH parr bomb	130C/100 %RH parr bomb	130C/100 %RH parr bomb
#1	0.3552	0.3625	0.3632	38K	M	M
#2	0.3624	0.3665	0.3596	M	M	M
#3	0.3584	0.3531	0.4825	0.45K	M	M
#4	0.3493	0.3508	0.6983	M	M	M
#5	0.3379	0.3429	M	M	M	M
#6	0.3422	0.9427	13.35	M	M	M
#7	0.3285	0.3313	0.8K	M	M	M
#8	0.3513	0.3487	348.13	0.51K	M	M
#9	0.3533	0.3596	0.3523	0.3624	0.3644	M
#10	0.3462	0.3511	0.3628	0.3584	M	M
#11	0.3742	0.3634	0.3553	0.3521	M	M
#12	0.3629	0.3638	0.3745	0.3678	M	M
#13	0.3585	0.3455	0.3658	0.3695	M	M
#14	0.3365	0.3452	0.3356	0.3328	16K	16K
#15	0.3277	0.3312	0.3188	0.3266	M	M
#16	0.3524	0.3489	0.3529	0.3514	0.3527	M

Figure 29: Cu-Al wire bond resistance values in Sample-1

The first part involves monitoring the change of resistance of interconnect using resistance spectroscopy (RS) under temperature humidity aging condition. The second part involves correlation of the location of the KCL drop inside the chip with the rate at which the Cu-Al wire bond fails. The final part involves making comparisons between

samples with built-in contaminant and their corresponding baseline samples. Resistance Spectroscopy [Lall 2012, 2013] has been shown to be a proven way to measure the change of the resistance accurately in both solder joints and wire bond interconnects. It is hypothesized that change of resistance of the Cu-Al wire bond can be used as a leading indicator to identify progression of damage and impending failure. The RS system consists of phase sensitive detection, modified Wheatstone bridge and a probe station. Accurate measurements can be obtained even when the signal is obscured by noise sources many times larger in magnitude. Lock-in amplifiers is designed to detect and measure very small AC signals all the way down to a few nanovolts.

# of PIN	Time zero	24 hr	48 hr	72hr	96hr
		130C/100 %RH parr bomb	130C/100 %RH parr bomb	130C/100 %RH parr bomb	130C/100 %RH parr bomb
#1	0.3721	0.3742	0.3623	0.3624	0.3556
#2	0.3588	0.3622	0.3672	0.3597	0.3564
#3	0.3562	0.3485	0.3464	0.3422	0.3442
#4	0.3648	0.3612	0.3688	0.3633	0.5839
#5	0.3413	0.3408	0.3514	0.3467	M
#6	0.3386	0.3356	0.3229	0.3319	M
#7	0.3378	0.342	0.3527	0.3462	M
#8	0.3744	0.3647	0.3632	0.3705	17.05
#9	0.3663	0.3635	0.3659	0.3559	M
#10	0.3574	0.3542	0.3541	0.3435	28.51
#11	0.3563	0.3521	0.3284	0.3541	M
#12	0.3662	0.3633	0.3781	0.3439	0.9026
#13	0.3682	0.3647	0.3562	0.3526	M
#14	0.345	0.3541	0.3447	0.3487	M
#15	0.3375	0.3372	0.3326	0.3335	8.56
#16	0.3629	0.3589	0.3663	0.3688	97.33

Figure 30: Cu-Al wire bond resistance values in Sample-2

It uses a technique known as phase-sensitive detection so as to single out the component of the signal at a specific reference frequency and phase. Operational details of the test technique can be found in [Lall 2012, 2013]. Resistance has been measured at an interval of 24 hours. Failure Threshold, according to the industry standard, is set to be the time when resistance exceeds 300 ohm [IPC-SM-785]. Wire bonds considered to be failed are highlighted with red (Figure 29, Figure 30) in spreadsheet and K and M denotes the resistance of wire bond reaches thousand and million level respectively. From analyzing the optical microscopic sample image #1 alone, one can guess that pin #6 is most likely to be corroded in the first place due to the fact that it is closest to the KCl drop thus is most susceptible one (Figure 28). After that, failure is going to happen on the pins around #6. Because of the distance between them and KCl drop is fairly close compare to the rest of the wire bonds, speculations are all verified by the resistance result of wire bonds that the failure initiated at pin#6 after 24hrs aging duration and then it spreads out to those wire bonds close to #6.

SUMMARY AND CONCLUSIONS

In this paper a multiphysics model for galvanic corrosion in the presence of chloride has been developed. The diffusion coefficients of chloride ion has been measured in the electrochemical molding compound at various temperatures using two methods including diffusion cell and inductively coupled plasma (ICPMS). Moisture ingress into the EMC has been quantified through measurements of the weight gain in the EMC as a function of time. Tafel parameters including the open circuit potential and the slope of the polarization curve has been measured for both copper, aluminum under different concentrations of the ionic species and pH values in the EMC. Electrochemical polarization tests on aluminum and copper indicates the galvanic corrosion between copper and aluminum is more likely to happen in the alkaline condition than in acidic condition. SEM/EDS analysis shows that the ionic diffusion in EMCs is due to interfacial diffusion and degradation of EMCs under high temperature results in the loss of binding materials. The contaminant diffusion along with the corrosion kinetics has been modeled. The measurements have been incorporated into the COMSOL model to predict the corrosion current at the Cu-Al bond pad. The model uses moving boundary to keep track of the development of corrosion as time proceeds. The model also show the gradual local alkalization at bond pad interface as the galvanic corrosion develops. The model predictions have been correlated with experimental data. In addition, contaminated samples with known concentration of KCl contaminant have been subjected to the temperature humidity conditions of 130°C/100RH. The resistance of the Cu-Al interconnects in the PARR test have been monitored periodically using resistance spectroscopy. Model predictions indicate that the pH values in the vicinity of the Cu-Al wirebond continue to evolve as a function of time.

ACKNOWLEDGMENTS

The work presented here in this paper has been supported by a research grant from the Semiconductor Research Corporation (SRC), Research ID 2284.

REFERENCES

- Bard, A.J., Faulkner, L.R., *Electrochemical Methods: Fundamentals and Applications*, Second Edition, John Wiley and Sons, 2001.
- Boettcher, T., Michael Rother Stefan Liedtke, Mandy Ullrich, Marc Bollmann, Andreas Pinkernelle, Daniel Gruber, Hans-Juergen Funke, Michael Kaiser, Kan Lee, Martin Li, Karina Leung, Tina Li, Mark Luke Farrugia, Orla O'Halloran, Matthias Petzold, Benjamin März, Robert Klengel, *On the Intermetallic Corrosion of Cu-Al wire bonds*, Proceedings of 12th Electronics Packaging Technology Conference, Singapore, pp.585-590, 2010
- Dunn, C.F., McPherson, J.W, *Recent Observations on Bond Pad Corrosion Kinetics*, *Electrochem. Soc.*, Vol. 135, No.3, pp.661-665, 1988.
- England, L. Siew Tze Eng., Chris Liew, Hock Heng Lim, *Cu-wire Bond Parameter Optimization On Various Bond Pad Metallization and Barrier Layer Material Schemes*, *Microelectronics Reliability*, Volume 51, No.1, pp.81-87, 2011
- Gan, C. L., F. C. Classe, B. L. Chan, U. Hashim, *Evolution and Investigation of Copper and Gold Ball Bonds in Extended Reliability Stressing*, *Gold Bulletin*, Volume 47, Issue 3, pp.141-151, September 2014.
- Iannuzzi, M, *Bias Humidity Performance and Failure Mechanisms of Non-hermetic Aluminum SIC's in an Environment Contaminated with Chloride Ions*, *IEEE Trans-CHMT*, Vol. 6, No.2, pp. 191-201, 1983.
- Jackson, S.E., Norman J. Pearson William L. Griffin, *The application of laser ablation-inductively coupled plasma mass spectrometry to in situ U-Pb zircon geochronology*, Volume 211, Issues 1–2, Pages 47–69, November 2004.
- Kilic, M.S., M.Z. Bazant, A. Ajdari, *Steric effects in the dynamics of electrolytes at large applied voltages. I. Double-layer charging*, *Physics Review*, E 75, pp. 021502-1 to 021502-16, 2007
- Kim, S.H., J.W. Park, S.J. Hong, J.T. Moon, *The Interface Behavior of the Cu-Al Bond System in High Humidity Conditions*, *Proceedings of 12th Electronics Packaging Technology Conference*, Singapore, pp.545-549, Dec 8-10, 2010
- Laik, A., K. Bhanumurthy, G.B Kale, *Diffusion in Cu (Al) Solid Solution*, *Defect and Diffusion Forum*, Volume 279, pp.63-69, August 2008.
- Lall, P., Lowe, R., Goebel, K., *Prognostication Based on Resistance-Spectroscopy and Phase-Sensitive Detection for Electronics Subjected to Shock-Impact*, *ASME J. Electron. Packag.* 134, 021001-1 to 021001-10, 2012.
- Lall, P., Luo, Y., *Resistance Spectroscopy Based Assessment of Degradation in Cu-Al Wire Bond Interconnects*, *Proceedings of the ASME 2013 International Technical Conference & Exposition on Packaging and Integration of Electronic and Photonic Microsystems*, InterPACK2013-73308, pp. 1-8, Burlingame, CA, 2013.
- Lantz, L., Pecht, M.G., *Ion Transport in Encapsulants Used in Microcircuit Packaging*, *IEEE Transactions on Components and Packaging Technologies*, Vol. 26, No.1, pp 199-205, March 2003
- Lee, Won-Bae, Kuek-Saeng Bang, Seung-Boo Jung, *Effects of intermetallic compound on the electrical and mechanical properties of friction welded Cu/Al bimetallic joints during annealing*, *Journal of Alloys and Compounds*, Vol. 390, Issues 1-2, pp 212–219, March 2005.
- Liu, H., Zhenqing Zhao, Qiang Chen, *Reliability of Copper Wire Bonding in Humidity Environment*, *Proceedings of the 13th Electronics Packaging Technology Conference*, Singapore pp.53-58, 2011.
- McCafferty, E., *Introduction to Corrosion Science*, Springer, 2010.
- Na, Seok Ho, TaeKyeong Hwang, JungSoo Park, JinYoung Kim, HeeYeoul Yoo and Choon Heung Lee, *Characterization of Intermetallic Compound (IMC) growth in Cu wire ball bonding on Al pad metallization*, *Proceedings of 61st IEEE Electronic Components and*

- Technology Conference, Lake Buena Vista, Florida, pp.1740-1745, May 31-June 3, 2011.
- Niu, H., R.S. Houk Fundamental Aspects of Ion Extraction in Inductively Coupled Plasma Mass Spectrometry, *Spectrochimica Acta Part B: Atomic Spectroscopy*, Vol. 51 Issue 8, pp. 779-815, 1996.
- Paulson, W.M., R.P. Lorain, Motorola Semiconductor Products Division, The effect of impurities on the corrosion of aluminum metallization, 14th Annual Reliability Physics Symposium, Las Vegas, NV, pp. 42-47, April 1976.
- Seki, Hidetoshi, Chen Ping, Hidetoshi Seki, Chen Ping, Hiroshi Nakatake, Shin-ichi Zenbutsu1, Shingo Itoh, Study of EMC for Cu bonding wire application, CPMT Symposium Japan, 2010 IEEE, Tokyo, pp.1-3, 24-26 Aug. 2010.
- Shen, C.H., G.S. Springer, Moisture absorption and Desorption of Composite Materials, *Journal of Composite Materials*, Vol.10, pp.2-20, 1976
- Van Soestbergen, M., L.J. Ernst, Transport of Corrosive Constituents in Epoxy Molding Compounds, 8th. Int. Conf. on Thermal, Mechanical and Multiphysics Simulation and Experiments in Micro-Electronics and Micro-Systems, IEEE EuroSimE pp. 42-47, 2007.
- Van Soestbergen, M., P.M. Biesheuvel, Modified Poisson-Nernst-Planck Theory for Ion Transport in Polymeric Electrolytes, *Journal of Electrostatics*, Vol 66, Issues 11-12, pp. 567-573, 2008
- Wieczorek-Ciurowa, K., K. Gamrat, Z. Sawlowicz, Characteristics of $\text{CuAl}_2\text{-Cu}_9\text{Al}_4/\text{Al}_2\text{O}_3$ Nanocomposites Synthesized by Mechanical Treatment, *Journal of Thermal Analysis and Calorimetry*, Vol. 80, pp.619-623, 2005.
- Wolff, F. W., C. D. Breach, and D. Stephan Characterization of Intermetallic Growth in Copper and Gold Ball Bonds on Aluminum Metallization; Proceedings of the Sixth EPTC Conference, pp. 348-353, 2004.